JACS
JOURNAL OF THE AMERICAN CHEMICAL SOCIETY
Article
pubs.acs.org/JACS

Superionic Phase Transition in Silver Chalcogenide Nanocrystals Realizing Optimized Thermoelectric Performance

Chong Xiao, Jie Xu, Kun Li, Jun Feng, Jinlong Yang, and Yi Xie*

Hefei National Laboratory for Physical Sciences at the Microscale, University of Science & Technology of China, Hefei, Anhui, 230026, P.R. China

Supporting Information

ABSTRACT: Thermoelectric has long been recognized as a potentially transformative energy conversion technology due to its ability to convert heat directly into electricity. However, how to optimize the three interdependent thermoelectric parameters (i.e., electrical conductivity σ, Seebeck coefficient S, and thermal conductivity κ) for improving thermoelectric properties is still challenging. Here, we put forward for the first time the semiconductor−superionic conductor phase transition as a new and effective way to selectively optimize the thermoelectric power factor based on the modulation of the electric transport property across the phase transition. Ultra low value of thermal conductivity was successfully retained over the whole investigated temperature range through the reduction of grain size. As a result, taking monodisperse Ag_2Se nanocrystals for an example, the maximized ZT value can be achieved around the temperature of phase transition. Furthermore, along with the effective scattering of short-wavelength phonons by atomic defects created by alloying, the alloyed ternary silver chalcogenide compounds, monodisperse Ag_4SeS nanocrystals, show better ZT value around phase transition temperature, which is cooperatively contributed by superionic phase transition and alloying at nanoscale.

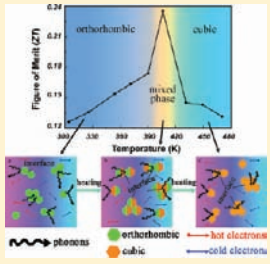

INTRODUCTION

The great energy demand for fossil fuels is steadily increasing to keep pace with the world economic growth. However, the conversion reactions required for retrieving energy from carbon resources bringing the production of green house gases and subsequent global warming effects, which significantly influence the Earth's environment today.[1] Therefore, efficient utilization of the energy has directed a global trend toward a diversified energy portfolio. On the basis of the conversion of heat into electricity, thermoelectric generators are today well recognized as viable renewable-energy sources.[2−5] The heat can come from the combustion of fossil fuels, from sunlight, or as a byproduct of various processes (e.g., chemical reactions, nuclear decay, and so on). Accordingly, thermoelectric materials can play a role in both primary power generation and energy conservation.

The performance of thermoelectric materials is quantified by a dimensionless figure of merit, ZT, which is defined as $\sigma \cdot S^2 T/\kappa$, where σ is the electrical conductivity, S is the Seebeck coefficient, κ is the thermal conductivity of the material, and T is the absolute temperature. The challenge to create high ZT thermoelectric materials lies in achieving simultaneously high σ, high S, and low κ in the same solid. However, there is a strong correlation of these three parameters according to the Wiedemann−Franz law; thus, materials development schemes to achieving superior thermoelectric materials and for subsequent practical application are driven by the need to maximize the figure of merit, ZT, and to balance the competing requirements of high Seebeck coefficient, high electrical conductivity, and low thermal conductivity.[6]

Over the past decades, most progress in thermoelectric materials has been made by reducing thermal conductivity through the introduction of soluble second phases,[7] mass fluctuation alloying,[8] or nanostructures such as quantum dots.[9−11] Many of these improvements are based on the increasing of interface or grain boundary for effective phonon scattering to reduce the thermal conductivity. However, while phonon scattering is significantly enhanced by these structures, the electron scattering is also enhanced, leading to a reduction in electrical conductivity, and thus the direct consequence is limited ZT improvement for thermoelectric materials. So, all three parameters are highly dependent on the details of the electronic structure and the charge carrier-related properties, and balancing the electronic and thermal properties is critical to tailor a material for optimal thermoelectric performance.

Occurrence of different polymorphic phases has often been observed in inorganic compounds, including natural and especially synthetic materials. Among them, many exhibit transformations from one crystal structure to another as the temperature or pressure is varied,[12] which is so-called phase transition. Besides such phase transitions involving changes in atomic configuration, many of the solids also undergo the orientation change of the electron clouds influencing the state of electron spin on passing through the phase transition, resulting in the widening/narrowing of the material bandgap to form insulator or metal states; this reveals an intriguing route to control the carrier concentration by modulating related effects of electronic properties.[13,14] Silver chalcogenides as typical materials with their intrinsic phase transition have attracted much interest due to, accompanied by the phase transition,

Received: November 12, 2011
Published: February 8, 2012

   dx.doi.org/10.1021/ja2104476 | J. Am. Chem. Soc. 2012, 134, 4287−4293

undergoing a reversible transformation between semiconductor and superionic conductor.[15−17] For example, Ag_2Se crystallizes in the orthorhombic phase at room temperature is a narrow-band gap semiconductor with two crystallographically distinct silver atoms,[18] while in the high-temperature cubic phase, α-Ag_2Se, selenium sublattice is ordered in a bcc lattice while silver atoms are statistically distributed over several interstitial sites,[19−22] through which Ag^+ cations can move easily and show superionic conductivity. As see in Figure 1, the calculated

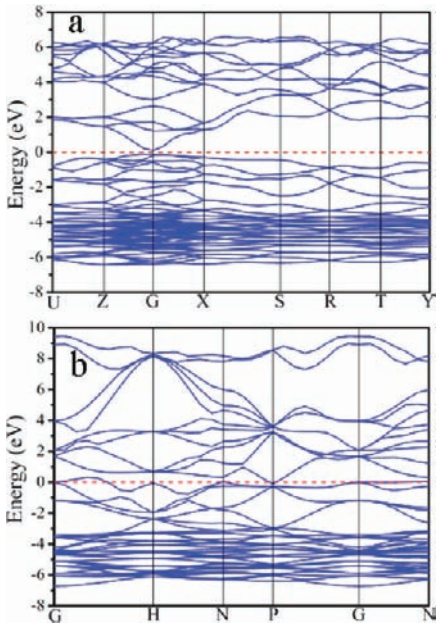

Figure 1. Calculated band structure of orthorhombic (a) and cubic (b) Ag_2Se respectively.

band gap is about 0.098 eV for orthorhombic Ag_2Se while 0 eV for cubic Ag_2Se which is consistent with the experimental finding that the high-temperature phase of Ag_2Se shows metallic behavior in its electronic conductivity. These two compounds undergo a reversible first-order phase transition around 406 K with a remarkable change in its electronic property, which is presently giving a hint for the modulation of the electric properties at the phase transition temperature to optimize thermoelectric power factor. Thus, one may expect to obtain superior thermoelectric property in these materials vicinal to their phase transition temperature.

In addition to the favorable electrical transport properties, a good thermoelectric material must also have low thermal conductivity (κ). A successful strategy to reduce the thermal conductivity has been applied to modify an already promising compound by reducing grain size to nanometer,[23−25] which serves to introduce a large density of interfaces in which mid/long-wavelength phonons can be effectively scattered. Although mid/long-wavelength phonons are effectively scattered in nanocrystals, the short-wavelength phonons can propagate without significant scattering and thereby still contribute to heat conduction. Alloying is another successful strategy to reduce thermal conductivity due to mass fluctuations in the crystal lattice and thus increase the short-wavelength phonon scattering to reduce the lattice thermal conductivity.[26−29] So, as a result of alloying at nanoscale, significant reduction in lattice thermal conductivity could be expected to be achieved since phonons with an approximately even distribution of wavelengths can be effectively scattered.

Herein we highlight a new pathway to successfully optimize the thermoelectric property in monodisperse Ag_2S, Ag_2Se, and Ag_4SeS nanocrystals. On the basis of the semiconductor−superionic conductor transition, the optimized power factor is obtained around the phase transition temperature. On the other hand, an ultralow value of thermal conductivity was successfully retained over the whole investigated temperature range through the reduction of grain size and Ag^+ ions disordering in the cubic phase. As a result, a maximized ZT value has been achieved around the phase transition temperature. Furthermore, the introduction of alloying into these superionic nanocrystals could further reduce the thermal conductivity, resulting in higher ZT value around the phase transition temperature. Our findings reveal that regulating the phase transition behavior in the superionic conductor with nanometer size allows advances in balancing the electronic and thermal properties, with remarkable promising signs for tailoring a material for optimal thermoelectric performance.

EXPERIMENTAL SECTION

Materials. All chemicals were of analytic grade purity obtained from Sinopharm Chemical Reagent Co., Ltd., and used as received without further purification.

Synthesis of Ag_2Se and Ag_2S Nanocrystals. Ag_2Se and Ag_2S nanocrystals were synthesized using a modification of the method proposed by Wang et al.[30] Briefly, 20 mL of octadecylamine was heated to 180 °C, and then 0.5 g of $AgNO_3$ was added. After the mixture was magnetically stirred for 10 min, 0.13 g of selenium or 0.06 g of sulfur powders was added into the system. The mixture was maintained at 180 °C for 3 h under stirring, and then the reaction was quickly stopped. The nanocrystals were separated from the resulting solution by centrifuge and washed several times with ethanol and cyclohexane. All the samples were dried in a vacuum at 60 °C for 6 h.

Synthesis of Ag_4SeS Nanocrystals. A total of 20 mL of octadecylamine was heated to 180 °C, and then 0.5 g of $AgNO_3$ was added. After the mixture was magnetically stirred for 10 min, 0.063 g of selenium and 0.026 g of sulfur powders were added into the system. The mixtures were maintained at 180 °C for 3 h under stirring, and then the reaction was quickly stopped. The nanocrystals were separated from the resulting solution by centrifuge and washed several times with ethanol and cyclohexane. All the samples were dried in a vacuum at 60 °C for 6 h.

Surfactants Removal Process and Bulk Samples Preparation. The organic surfactants were removed via the procedure of previously reports[31] before fabrication of bulk samples for thermoelectric measurement. Briefly, as-prepared silver chalcogenides were dispersed in cyclohexane with hydrazine solution (85% v/v) and stirring vigorously until all the nanocrystals were precipitated. The supernatant was decanted, and the precipitate was washed with ethanol three times to remove hydrazine, collected by centrifugation, and then dried in vacuum at 65 °C. After the hydrazine treatment, the nanocrystals were hot-pressed into rectangular (10 mm ×4 mm ×1.5 mm) and round disk bulk samples (with diameter of about 13 mm and thickness of 2 mm) under 60 MPa at 400 °C for 30 min.

Characterization. The structure of these obtained samples was characterized with the X-ray diffraction (XRD) pattern, which was recorded on a Rigaku Dmax diffraction system using a Cu Kα source (λ = 1.54187 Å). X-ray photoelectron spectroscopy (XPS) measurements were performed on a VGESCALAB MK II X-ray photoelectron spectrometer with an excitation source of Mg Kα = 1253.6 eV. Electron microscopy observations were carried out with a Hitachi H-800 transmission electron microscope at 100 kV. High-resolution transmission electron microscopy (HRTEM) images were performed on JEOL-2010 transmission electron microscope at 200 kV. Variable-temperature XRD patterns of the samples were recorded following

dx.doi.org/10.1021/ja2104476 | J. Am. Chem. Soc. 2012, 134, 4287−4293

both heating and cooling protocols between 298 and 473 K by the Shimadzu XRD-7000 with Cu Kα radiation (λ = 1.54187 Å). DSC cycling curves were measured by the NETZSCH DSC Q2000 with a heating/cooling rate of 5 K min^{-1} between 273 and 480 K.

Thermoelectric Properties. Rectangular shape samples with typical sizes of 10 mm × 4 mm × 1.5 mm were employed to simultaneously measure Electrical conductivity σ and Seebeck coefficient S by the standard four-probe methods in a He atmosphere (ULVAC-RIKO ZEM-3). Thermal conductivity κ was calculated using the equation $\kappa = a\rho C_p$ from the thermal diffusivity obtained by a flash diffusivity method (LFA 457, Netzsch) on a round disk sample with diameter of about 13 mm and thickness of 2 mm, specific heat C_p determined by a differential scanning calorimeter method (DSC Q2000, Netzsch).

Calculation Details. The band structure calculations of orthorhombic and cubic Ag_2Se were performed using the CASTEP program package with the Perdew-Burke-Ernzerhof (PBE) GGA functional.

RESULTS AND DISCUSSION

Inspired by the above structural and electronic band structure analysis, we selected silver chalcogenides as examples for the investigation of phase transition with remarkable electronic property change on their thermoelectric property. Monodisperse silver chalcogenides nanocrystals with narrow size distribution were synthesized through a simple colloidal method. The phase purity and crystal structure of the as-prepared products were examined by XRD, and the results are shown in Figure 2a. The XRD pattern of Ag_2Se matches well

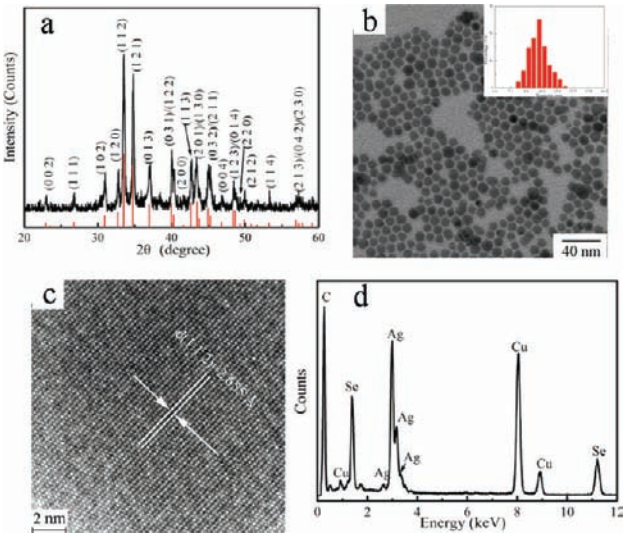

Figure 2. XRD pattern (a), TEM image (b), HRTEM image (c), and EDX spectrum (d) for as-prepared Ag_2Se nanocrystals.

with the standard orthorhombic Ag_2Se (space group: $P2_12_12_1$) with lattice constants a = 4.333 Å, b = 7.062 Å, and c = 7.764 Å (JCPDS 24-1041). The shape or morphology of pristine nanocrystals was examined by TEM and HRTEM. As shown in Figure 2b, we can see the Ag_2Se nanocrystals sized in an average diameter of 10 nm with hexagonal shapes. The TEM images also display the nearly monodisperse particle size distributions (see the inset of Figure 2b). The HRTEM images (Figure 2c) of one individual nanocrystal indicated the distances between the adjacent lattice fringes to be 2.655 Å which corresponds with the lattice spacing of the (112) d-spacing for orthorhombic Ag_2Se (2.673 Å, JCPDS 24-1041). Energy dispersive X-ray emission spectra (EDX) were measured to study the elemental composition and purity of these as-obtained products. The EDX results shown in Figure 2d undoubtedly demonstrate that the chemical components only consisted of Ag and Se for the as-obtained nanocrystals. As shown in Figure 2d, no other elemental species can be detected, indicating the high purity of these samples (the other detected elements Cu and C originated from the carbon-coated copper grid used for the TEM analysis). Direct experimental information for the composition and the purity of the products were also examined by XPS (Figure S1, Supporting Information), as well as the EDX results. They both experimentally verified the high purity of these samples.

The first-order phase transition usually involves a substantial entropy component, and our thermal analysis studies reveal the direct character of the first-order structural transition in solid materials. Typically, the appearance of endothermic (peak centered around 408 K) and exothermal (peak centered around 379 K) peaks in DSC curves (see in Figure 3a) during the

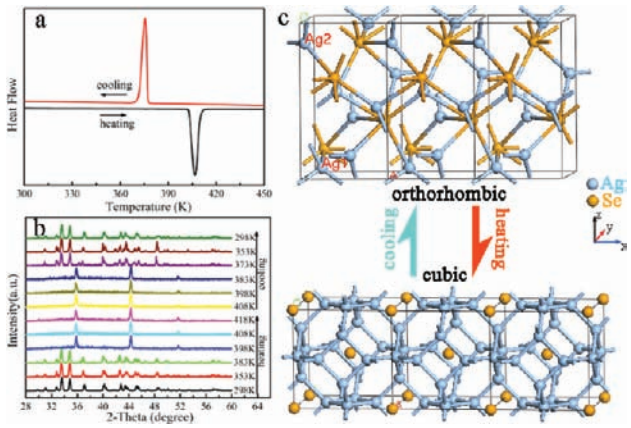

Figure 3. DSC thermogram (a), temperature-dependent XRD patterns (b) of the as-prepared Ag_2Se nanocrystals, and (c) schematic representation of the structure phase transition between orthorhombic and cubic Ag_2Se.

heating and cooling process clearly confirms the first-order transition of orthorhombic Ag_2Se. Detailed insight into the phase transition behavior of Ag_2Se nanocrystals was obtained from the temperature-dependent XRD. Results of the variable temperature XRD measurements for obtained products are shown in Figure 3b. It can be seen that the as-prepared Ag_2Se samples clearly show the structural transition from the low-temperature orthorhombic phase to the high-temperature cubic phase. In fact, Ag_2Se is a narrow band gap semiconductor and crystallizes in the orthorhombic phase at room temperature with two crystallographically distinct silver atoms:[32,33] Ag(1) is coordinated tetrahedrally, whereas the coordination sphere of Ag(2) is almost triangular (Figure 3c). In the high-temperature cubic phase, selenium sublattice is ordered in a bcc lattice while silver atoms are statistically distributed over several interstitial sites and delocalized in the channels along [100] consisting of octahedral and tetrahedral sites, through which Ag^+ cations can move easily and show superionic conductivity.[19,34−36] Furthermore, as shown in Figure S2 (Supporting Information), the mixed orthorhombic and cubic phases existed in temperature ranges of 403−413 K which would be attributed to the reduction of the lattice thermal conductivity.

It is well-known that Ag_2Se is a narrow band gap semiconductor and promising candidate for the potential application of thermoelectric devices thanks to their high

dx.doi.org/10.1021/ja2104476 | J. Am. Chem. Soc. 2012, 134, 4287−4293

electrical conductivity and relatively high Seebeck coefficient. For the thermoelectric properties measurement, we have carefully removed the organic surfactants according to the procedure of previous reports and fabricated the hot-pressed bulk samples (the XRD patterns and SEM images of surface cleaned and hot-pressed bulk samples are shown in Figure S3, Supporting Information). As shown in Figure S3a, there are no apparent changes of structure and purity of the samples was detected after hydrazine treatment and hot-pressing compared to the pristine nanocrystals. The SEM image (Figure S3b) of Ag_2Se nanocrystals clearly showed that the size and shape were almost unchanged after hydrazine treatment, and also the bulk sample consisting of hot-pressed (Figure S3c) Ag_2Se nanocrsytals are very dense with smooth surface. Figure 4 shows the

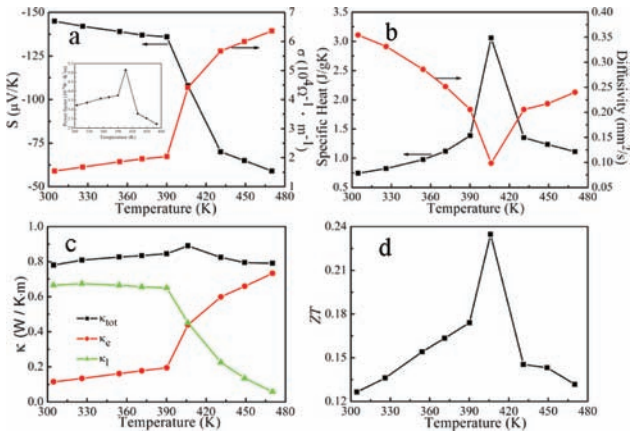

Figure 4. (a) Temperature dependence of the Seebeck coefficient (black) and the electrical conductivity (red) for Ag_2Se nanocrystals. (b) Evolution of the specific heat (black) and of the thermal diffusivity (red) of Ag_2Se nanocrystals as a function of temperature. (c) Temperature dependence of thermal conductivity for Ag_2Se nanocrystals. (d) Temperature dependence of the thermoelectric figure of merit ZT for Ag_2Se nanocrystals.

thermoelectric property of the hot-pressed Ag_2Se sample. As shown in Figure 4a, a pronounced increase in electric conductivity with temperature increasing to near 408 K clearly shows the typical electrical transition originated from the atom rearrangement and Ag^+ disordering during the structural transition. As it is known, the low-temperature Ag_2Se phase belongs to the orthorhombic system and has semiconducting properties with degenerate state of the electron gas, and then the low-temperature Ag_2Se phase changes to cubic type and exhibits a superionic conductivity behavior as temperature increased. Figure 4a also shows the Seebeck coefficient of these as-prepared nanocrystals. The negative sign of the Seebeck coefficient indicates that Ag_2Se nanocrystals are n-type semiconductor, and as temperature increased, the Seebeck coefficient (absolute value) dropped from 150 μV/K to 60 μV/K around 408 K. It is well-known that the electrical conductivity is proportional to the charge carrier concentration, while the Seebeck coefficient decreases with increasing charge carrier concentration.[37−40] As a result, the metals usually display Seebeck coefficients of a few tens of μV/K which are much lower than that of semiconductors. So, in this study, the larger Seebeck coefficient of low temperature phase and lower Seebeck coefficient of high temperature should be an inevitable result of the semiconductor−superionic conductor phase transition. Results revealing that the presence of structural phase transition concomitant with the abrupt increase in electrical conductivity by several orders of magnitude at elevated temperature affords the chance to balance the electronic and thermal properties around the transition temperature for achieving superior thermoelectric performance. On the basis of the regulation of electric transport property, a maximum power factor (σS^2) is obtained around the phase transition temperature (see inset of Figure 4a), which is a crucial step toward improving thermoelectric properties.

In addition to having favorable electrical transport properties, a good thermoelectric material must also have low thermal conductivity (κ). Figure 4c displays the temperature dependence of the thermal conductivity κ. Of exciting, the thermal conductivity of Ag_2Se nanocrystals is much lower than those of many reported thermoelectric materials and covers the range of 0.78 to 0.89 W/mK over the temperature range of 300 to 480 K. A tiny peak in the thermal conductivity occurs, which is caused by the abrupt change of the silver ion mobility around orthorhombic−cubic phase transition temperature at 408 K. Although the increase of thermal conductivity is disadvantageous to obtaining a high figure of merit, the absolute value is still much lower compared with the previously reported values. The thermal conductivity was calculated by the following eq 1

$$\kappa = a\rho C_p \tag{1}$$

using the measured heat capacity C_p, the measured thermal diffusivity a, and the density ρ. A huge λ-shaped effect in the C_p curve (Figure 4b) comes along with the phase transition at 408 K featuring a heat capacity maximum of 3.06 J/(g K). Surprisingly, the thermal diffusivity (see in Figure 4b) is low and covers the range of 0.098 to 0.35 mm^2/s over the temperature range of 300 to 480 K. At the orthorhombic−cubic phase transition, a significant reduction of the thermal diffusivity to a very low value of 0.098 mm^2/s at 408 K occurs that substantiated the huge mobility of the silver cations and the rearrangement of the anions during the transition.

As is known, κ is the sum of two independent components, a lattice contribution κ_l and an electronic contribution κ_e equal to LT/ρ according to the Wiedemann−Franz law (L is the Lorenz constant and equal to 2.45×10^{-8} $W\cdot\Omega\cdot K^{-2}$). At low temperature, Ag_2Se is a semiconductor with relatively low electrical conductivity, and electrical contribution to the total thermal conductivity may be neglected, while the lattice thermal conductivity is also very low due to the reduction of grain size. Theoretically, reduction to nanometer grain size serves to introduce a large density of interfaces in which phonons can be effectively scattered resulting in the reduction of lattice thermal conductivity without having to compromise carrier mobility values (see in Scheme 1a).[41]

As temperature increased to 408 K, the orthorhombic to cubic phase transition appeared. Along with the phase transition, Ag_2Se began the change from semiconductor to superionic conductor and the electrical conductivity sharply increased. Although the electrical contribution to total thermal conductivity could not be neglected during the phase transition, the lattice thermal conductivity dropped contrarily but acutely. It is well-known that during the phase transition, the parent phase disappeared gradually while the secondary phase appeared. In our case, the in situ formed nanostructured Ag_2Se cubic phase evenly coexists with the orthorhombic phase (which could be testified by the temperature-dependent XRD, as seen in Figures 3b and S2, Supporting Information), making our samples in situ nanocomposites (see in Scheme 1b). The

dx.doi.org/10.1021/ja2104476 | J. Am. Chem. Soc. 2012, 134, 4287−4293

Scheme 1. Schematic Diagram Illustrating Various Phonon Scattering Mechanisms in Ag_2Se Nanocrystals[a]

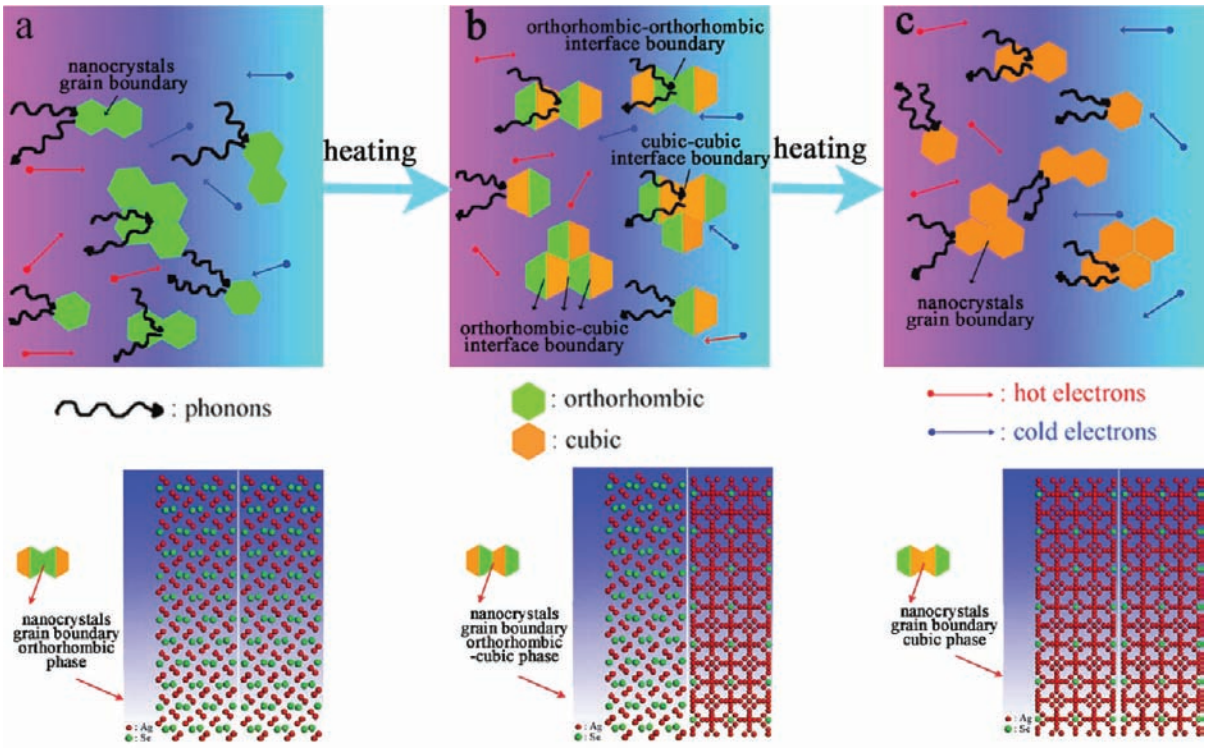

[a](a) Before phase transition, (b) during phase transition, and (c) after phase transition.

abundance of nanointerfaces effectively increases the phonon scattering and hence reduces the lattice thermal conductivity.[42] So, due to the combined contribution from electron and lattice, the total thermal conductivity gradually and slowly increases to 0.89 W/mK during the phase transition.

As temperature further increased to above the phase transition region, the Ag_2Se crystallizes in the cubic phase. In the high-temperature cubic phase, the anion sublattice is ordered in a bcc lattice while silver atoms are statistically distributed over several interstitial sites. It was found that the silver cations are delocalized in channels along [100] consisting of octahedral and tetrahedral sites, through which Ag^+ cations can move easily and show high conductivity. Due to the disordering of Ag^+ cations in the lattice, the phonons could be effectively scattered, which preserve the low lattice thermal conductivity. So, although there is a slight increase of total thermal conductivity through the phase transition, the value is still retained at a very low level over the investigated temperature range, which may be contributed by the Ag^+ disordering and nanostructing.

In Figure 4d, the figures of merit for Ag_2Se nanocrystals calculated from the above data with the relationship $\sigma \cdot S^2T/\kappa$ are shown. Of note, the Ag_2Se nanocrystals achieve a maximum $ZT_{max} = 0.23$ at the phase transition temperature around 408 K, which is reminiscent of the features of the temperature-dependent power factor curve. Our figure of merit behavior confirms the ability to achieve the thermoelectric materials with balanced electrical conductivity and lattice thermal conductivity through the intrinsic phase transition. Moreover, the optimized thermoelectric property obtained around phase transition temperature was confirmed as a general law rather than an individual case, as, in another example, 12 nm of monodisperse Ag_2S nanocrystals (for details information of structural, size, and morphology see Figure S4, Supporting Information) also possesses a maximum ZT value of 0.12 around its semiconductor−superionic conductor phase transition temperature at 454 K.

To further lower the thermal conductivity, it is necessary to reduce the phonon mean free path. A successful strategy to reduce thermal conductivity is the design of alloys to create point defects that scatter heat carrying phonons. The introduction of randomness in the lattice by alloying often results in sufficient disorder or point defects to produce phonon scattering and is of great importance in the improvement of the performance of thermoelectric materials. So, the thermoelectric property of alloyed ternary silver chalcogenide compound, Ag_4SeS, was also investigated. In this study, monodisperse Ag_4SeS nanocrystals were successfully synthesized for the first time. All the diffraction peaks of XRD patterns in Figure 5a can be exclusively indexed as the orthorhombic Ag_4SeS (space group: $P2_12_12_1$) with lattice constants a = 4.33 Å, b = 7.09 Å, and c = 7.76 Å (JCPDS 27-0620). No peaks attributable to impurities were observed, indicating the high purity of as-obtained products. The relatively broad peaks in the diffraction patterns were consistent with their small sizes. The shape or morphology of these nanocrystals was examined by TEM and HRTEM. As shown in Figure 5b, we can see the Ag_4SeS nanocrystals sized in an average diameter of 13 nm with hexagonal shapes. The TEM images also display the nearly monodisperse particle size distributions (see the inset of Figure 5b). The HRTEM images (Figure 5c) of one individual nanocrystal indicated the distances between the adjacent lattice fringes to be 2.428 Å which corresponds with the lattice spacing of the (013) d-spacing of Ag_4SeS (2.430 Å, JCPDS 27-0620). The EDX results shown in Figure 5d undoubtedly demonstrate that the chemical

dx.doi.org/10.1021/ja2104476 | J. Am. Chem. Soc. 2012, 134, 4287−4293

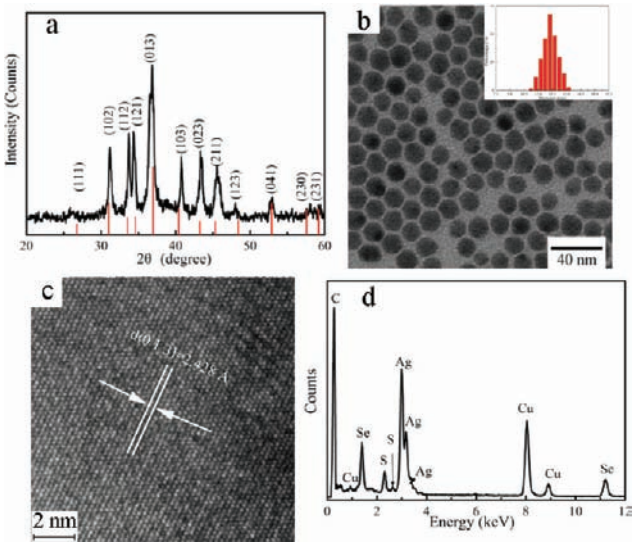

Figure 5. XRD pattern (a), TEM image (b), HRTEM image (c), and EDX spectrum (d) for as-prepared Ag_4SeS nanocrystals.

components only consist of Ag, Se, and S with a Se to S atomic ratio of nearly 1:1. No other elemental species can be detected, indicating the high purity of these samples (the other detected elements Cu and C are originated from the carbon-coated copper grid used for the TEM analysis).

Compared to the binary silver chalcogenide compounds, the phase transition temperature of monodisperse alloyed ternary silver chalcogenide Ag_4SeS nanocrystals was depressed to 355 K. It can be seen that the phase transition is indeed reversible in DSC curves (see in Figure S5, Supporting Information): a dominant endothermic peak is centered around 355 K during heating, and an exothermic peak is centered at 331 K. The introduction of randomness in the lattice by alloying often results in sufficient disorder or defect (see in Figure S6, Supporting Information) to produce phonon scattering and is of great importance in the improvement of the performance of thermoelectric materials, and the scattering cross-section follows Rayleigh scattering as d^6/λ^4. Hence, short-wavelength phonons are effectively scattered in alloys. Our results (see Figure 6 and Table 1) strongly suggest that the atomic disorder between the Se and the S atoms connected with the nanostructing which scatters the mid/long wavelength phonons should be responsible for the reduction of the lattice thermal conductivity in the Ag_4SeS solid solution alloy: the thermal conductivity maintains a very low value and covers a range of 0.64 to 0.71 W/mK over a temperature range of 300 to 480 K. The figures of merit for Ag_4SeS nanocrystals calculated from the above data with the relationship $\sigma \cdot S^2 T/\kappa$ are shown. Of note, the Ag4SeS nanocrystals achieve maximum $ZT_{max} = 0.33$ at the phase transition temperature around 355 K.

CONCLUSION

In summary, nearly monodisperse silver chalcogenide nanocrystals were successfully synthesized through a facile colloidal method, and their thermoelectric property across the semiconductor−superionic conductor phase transition was systematically investigated for the first time. Our findings reveal that regulating the phase transition behavior coupled with reduced grain size in solids allows advances in balancing the electronic and thermal properties for optimal thermoelectric properties. As a consequence, a maximized ZT was achieved around the

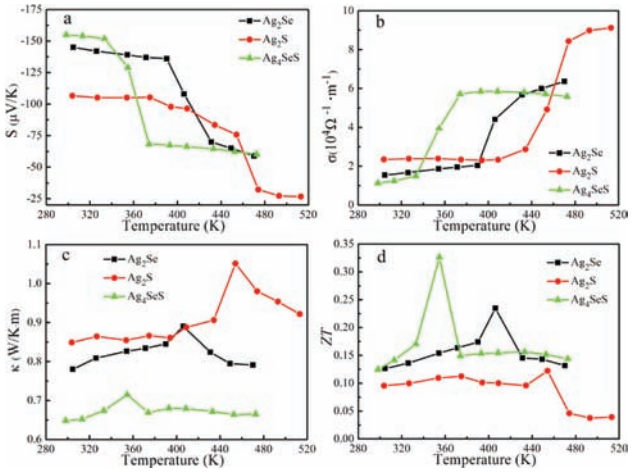

Figure 6. Temperature dependence of the Seebeck coefficient (a), electrical conductivity (b), thermal conductivity (c), and thermoelectric figure of merit ZT (d) for Ag_2S, Ag_2Se, and Ag_4SeS nanocrystals, respectively.

Table 1. Summary of Seebeck Coefficient, Electrical Conductivity, Thermal Conductivity, and Thermoelectric Figure of Merit ZT at Phase Transition Temperature for Ag_2S, Ag_2Se, and Ag_4SeS nanocrystals

sample	transition temperature (T_t, K)	S at T_t (μV/K)	σ at T_t (10^4 Ω·m)	κ at T_t (W/mK)	ZT at T_t
Ag_2S	454	−75.8	4.92	1.05	0.12
Ag_2Se	408	−108	4.41	0.89	0.23
Ag_4SeS	355	−129	3.95	0.71	0.33

temperature of the semiconductor−superionic conductor transition. Furthermore, along with the effective scattering of short-wavelength phonons by atomic defects created by alloying, the alloyed ternary silver chalcogenide compounds Ag_4SeS show much lower thermal conductivity and better ZT value around the phase transition temperature, which is cooperatively contributed by semiconductor−superionic phase transition, reduction of grain size, and alloying. This work inspires us that taking advantage of the cooperative contribution of superionic phase transition, reduced grain size, and alloying opens up a promising new approach to tailor materials for optimal thermoelectric performance.

ASSOCIATED CONTENT

Supporting Information

XPS for Ag_2S, Ag_2Se, and Ag_4SeS nanocrystals. Variable-temperature XRD patterns of Ag_2Se nanocrystals. XRD patterns and SEM images of Ag_2Se nanocrystals after surfactant removal and hot-pressing. XRD pattern, TEM and HRTEM images, and EDX for Ag_2S nanocrystals. DSC curve of Ag_4SeS nanocrystals. Phonons scattering mechanism for Ag_4SeS nanocrystals. Temperature dependence of κ, κ_l, and κ_e for Ag_4SeS and Ag_2S nanocrystals. This material is available free of charge via the Internet at http://pubs.acs.org.

AUTHOR INFORMATION

Corresponding Author

yxie@ustc.edu.cn

Notes

The authors declare no competing financial interest.

■ ACKNOWLEDGMENTS

This work was financially supported by National Basic Research Program of China (No. 2009CB939901), National Natural Science Foundation of China (11079004, 90922016, 10979047, J1030412), innovation project of Chinese Academy of Science (KJCX2-YW-H2O).

■ REFERENCES

(1) Wise, M.; Calvin, K.; Thomson, A.; Clarke, L.; Bond-Lamberty, B.; Sands, R.; Smith, S. J.; Janetos, A.; Edmonds, J. *Science* **2009**, *324*, 1183.
(2) Heremans, J. P.; Jovovic, V.; Toberer, E. S.; Saramat, A.; Kurosaki, K.; Charoenphakdee, A.; Yamanaka, S.; Snyder, G. J. *Science* **2008**, *321*, 554.
(3) Johnsen, S.; He, J. Q.; Androulakis, J.; Dravid, V. P.; Todorov, I.; Chung, D. Y.; Kanatzidis, M. G. *J. Am. Chem. Soc.* **2011**, *133*, 3460.
(4) Yu, J.-K.; Mitrovic, S.; Tham, D.; Varghese, J.; Heath, J. R. *Nat. Nanotechnol.* **2010**, *5*, 718.
(5) Snyder, G. J.; Toberer, E. S. *Nat. Mater.* **2008**, *7*, 105.
(6) Kanatzidis, M. G. In *Semiconductors and Semimetals*; Terry, M. T., Ed.; Elsevier: Amsterdam, 2001; Vol. *69*, p 5.
(7) Hyun, D. B.; Hwang, J. S.; Shim, J. D.; Oh, T. S. *J. Mater. Sci.* **2001**, *36*, 1285.
(8) Culp, S. R.; Simonson, J. W.; Poon, S. J.; Ponnambalam, V.; Edwards, J.; Tritt, T. M. *Appl. Phys. Lett.* **2008**, *93*, 022105.
(9) Harman, T. C.; Taylor, P. J.; Walsh, M. P.; LaForge, B. E. *Science* **2002**, *297*, 2229.
(10) Wang, R. Y.; Feser, J. P.; Lee, J. S.; Talapin, D. V.; Segalman, R.; Majumdar, A. *Nano Lett.* **2008**, *8*, 2283.
(11) Venkatasubramanian, R.; Siivola, E.; Colpitts, T.; O'Quinn, B. *Nature* **2001**, *413*, 597.
(12) Rao, C. N. R. *Acc. Chem. Res.* **1984**, *17*, 83.
(13) Imada., M.; Fujimori., A.; Tokura., Y. *Rev. Mod. Phys.* **1998**, *70*, 1039.
(14) Wu, C. Z.; Feng, F.; Feng, J.; Dai, J.; Peng, L. L.; Zhao, J. Y.; Yang, J. L.; Si, C.; Wu, Z. Y.; Xie, Y. *J. Am. Chem. Soc.* **2011**, *133*, 13798.
(15) Junod, P. *Helv. Phys. Acta* **1959**, *32*, 567.
(16) Kobayashi, M. *Solid State Ionics* **1990**, *39*, 121.
(17) Santhosh Kumar, M. C.; Pradeep, B. *Semicond. Sci. Technol.* **2002**, *17*, 261.
(18) Ge, J. P.; Xu, S.; Liu, L. P.; Li, Y. D. *Chem.—Eur. J.* **2006**, *12*, 3672.
(19) Boolchand, P.; Bresser, W. J. *Nature* **2001**, *410*, 1070.
(20) Utsugi, Y. *Phys. Rev. B* **1997**, *55*, 10800.
(21) Hamilton, M. A.; Barnes, A. C.; Howells, W. S.; Fischer, H. E. *J. Phys.: Condens. Matter* **2001**, *13*, 2425.
(22) Oliveria, M.; McMullan, R. K.; Wuensch, B. J. *Solid State Ionics* **1988**, *28*−*30*, 1332.
(23) Cook, B. A.; Kramer, M. J.; Harringa, J. L.; Han, M.; Chung, D. Y.; Kanatzidis, M. G. *Adv. Funct. Mater.* **2009**, *19*, 1254.
(24) Zhao, Y. X.; Dyck, J. S.; Hernandez, B. M.; Burda, C. *J. Am. Chem. Soc.* **2010**, *132*, 4982.
(25) Son, J. S.; Park, K.; Han, M. K.; Kang, C. Y.; Park, S. G.; Kim, J. H.; Kim, W.; Kim, S. J.; Hyeon, T. *Angew. Chem., Int. Ed.* **2011**, *50*, 1363.
(26) Ioffe, A. *Semiconductors Thermoelements and Thermoelectric Cooling*; Infosearch Ltd.: London, 1957.
(27) Chung, D. Y.; Hogan, T.; Brazis, P.; Rocci-Lane, M.; Kannewurf, C.; Bastea, M.; Uher, C.; Kanatzidis, M. G. *Science* **2000**, *287*, 1024.
(28) Wölfing, B.; Kloc, C.; Teubner, J.; Bucher, E. *Phys. Rev. Lett.* **2001**, *86*, 4350.
(29) Hsu, K. F.; Loo, S.; Guo, F.; Chen, W.; Dyck, J. S.; Uher, C.; Hogan, T.; Polychroniadis, E. K.; Kanatzidis, M. G. *Science* **2004**, *303*, 818.
(30) Wang, D. S.; Xie, T.; Peng, Q.; Li, Y. D. *J. Am. Chem. Soc.* **2008**, *130*, 4016.
(31) Scheele, M.; Oeschler, N.; Meier, K.; Kornowski, A.; Klinke, C.; Weller, H. *Adv. Funct. Mater.* **2009**, *19*, 3476.
(32) Wiegers, G. A. *Am. Mineral.* **1971**, *56*, 1882.
(33) Billetter, H.; Ruschewitz, U. *Z. Anorg. Allg. Chem.* **2008**, *634*, 241.
(34) Utsugi, Y. *Phys. Rev. B* **1997**, *55*, 10800.
(35) Hamilton, M. A.; Barnes, A. C.; Howells, W. S.; Fischer, H. E. *J. Phys.: Condens. Matter* **2001**, *13*, 2425.
(36) Oliveria, M.; McMullan, R. K.; Wuensch, B. J. *Solid State Ionics* **1988**, *28*−*30*, 1332.
(37) Bux, S. K.; Fleurial, J. P.; Kaner, R. B. *Chem. Commun.* **2010**, *46*, 8311.
(38) Kleinke, H. *Chem. Mater.* **2010**, *22*, 604.
(39) Shakouri, A. *Annu. Rev. Mater. Res.* **2011**, *41*, 399.
(40) Tritt, T. M. *Annu. Rev. Mater. Res.* **2011**, *41*, 433.
(41) Bux, S. K.; Fleurial, J.-P.; Kaner, R. B. *Chem. Commun.* **2010**, *46*, 8311.
(42) Urban, J. J.; Talapin, D. V.; Shevchenko, E. V.; Kagan, C. R.; Murray, C. B. *Nat. Mater.* **2007**, *6*, 115.